

Electro-mechanical modeling of a deicing device for aeronautics application

Melissa ESTOPIER CASTILLO^{1,2}, Thanh Trung NGUYEN^{1,2}, Edith CLAVEL^{1,2}, Nicolas GALOPIN^{1,2}, Frédéric WURTZ^{1,2}, Stéphane LE GARREC³

¹Université Grenoble Alpes, G2Elab, F-38000 Grenoble, FRANCE

²CNRS, G2Elab, F-38000 Grenoble, FRANCE

³ZODIAC AEROSPACE, CS20001 - 78373 – Plaisir, FRANCE

melissa.estopier-castillo@g2elab.grenoble-inp.fr

ABSTRACT— This paper address the multiphysical modeling for a new electromechanical deicing device. The technology proposed by aeronautics industry is based on the deformation of a plate subjected to magnetic forces action. Electro-magneto-mechanical modeling is intended for expressing the interdependence between the mechanical response and the electrical stimulus. The resulting expressions incorporate the dynamics of the response and the particular topology of the structural elements of the device. Measurements from previous prototypes served to validate the final model. As the goal was to obtain a model adapted for optimization process, some results and perspectives are also discussed.

Index Terms— aeronautics, deicing, electro-mechanical modeling, Laplace forces, plate deformation.

1. INTRODUCTION

Aeronautics industry is currently working to design a more electric aircraft. Research includes innovative solutions to reconceive all the systems that constitute an airplane in order to convert them into 100% electric [1]. Concerning flight safety, different solutions to icing problem already exist and are classified in two categories, anti-icing and deicing systems. However, they often present high energy consumption and large volume disadvantages.

A new electro-mechanical deicing solution for the wing edges of airplanes is proposed by our industrial associate “Zodiac Aerospace”. This technology is based on the repulsion effect between two electric conductors due to the circulation of opposite-sense currents. The device is inserted over the wing structure and right under the abrasion shield of the wing, as illustrated in figure 1. While one of the conductors is fixed to the plane structure, the other is nearly close to the internal face of the aluminum abrasion shield. When high intensity currents are applied to the conductors, the forces generated make the upper conductor get in contact with the abrasion shield brutally deforming it. Deformation takes place always within the elastic zone of the materials. Hence the ice is broken and the air flow takes away the remaining particles [2].

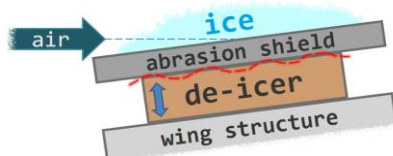


Fig.1 Electromechanical deicer array [2].

The purpose of this work is to construct a mathematical model with the characteristics of the experimental device to better understand the influence of the design parameters of the system over the total deformation. Once the model is achieved and validated, it is possible to start the sensibility testes and select the optimization algorithm that will permit obtaining the values for the geometrical and electrical entries of the deicer that guarantee the maximal deformation, minimizing the energy consumption per surface unit.

Development of a multiphysical model was achieved by analyzing in parallel the different study areas and putting them together as there are complementary. Firstly, it was necessary to depict the device construction and the technical specifications. Then, the electromechanical model was coordinated to the development of the electrical analysis. In a second time, mechanical model definition was launched; starting with a simplistic beam deflection approach that was later neglected because of the lack of accuracy. At the end, the plate deformation mechanical model is retained as it proved to be representative of the deicer behavior. So, the models were put together, enhanced by mutual consonance, and refined in a unique final model. All these project stages are going to be explained next.

2. ELECTROMECHANICAL DEICER

The system is composed of two layers of electric conductors placed face to face, as it can be appreciated in figure 2. Conductors section is rectangular. In the midst of these two spires, a polyamide panel containing numerous elastomer cylindrical inserts is disposed. These elements act as springs that ensure recovering of the initial position after activation. The whole structure is packed within a polyamide film to be later vulcanized in the intention of maintaining all the parts together, giving support and providing electrical isolation. Final device has a parallelepiped form with longitude b , width a and about 1mm thick.

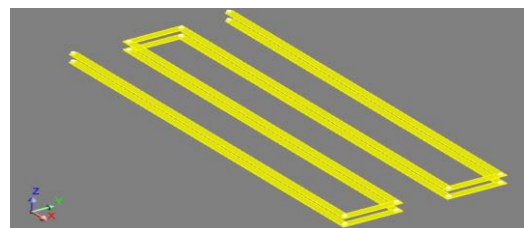


Fig.2 Layout of the two series of conductors.

From the electrical point of view, the intensity of the current impulse is about 4kA to 10kA, generated by a high value capacitors discharge, 800 μ F-2000 μ F, previously charged up to 400 and 800 V. Capacitors should be later replaced by a dedicated power source, though its development will not be treated in this paper. The electric activation signal is presented in figure 3, with an activation peak of 50 μ s length.

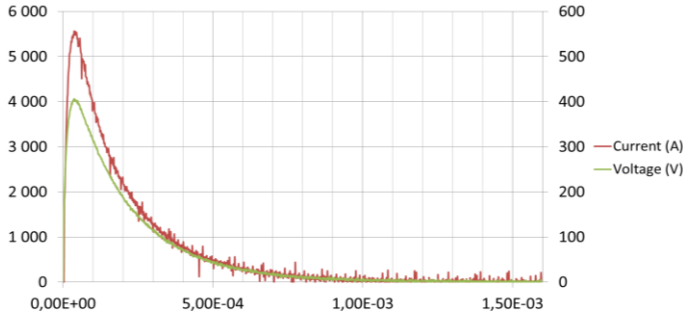


Fig. 3 Current and voltage activation impulse [4].

As mentioned before, the ice is broken as a consequence of the abrasion shield deformation. It has been proven that for deicing a plane surface or a flexible thin shield, it is effective to flex the regarding surface minimizing the ice breaking constraints [3].

Geometry, size, activation time and other crucial considerations for flying conditions, as for example Panchen's Law analysis [4], were determined and justified by our industrial partner in previous studies [5,6].

3. ELECTRO-MECHANICAL MODELING

The modeling of this actuator involved a multiphysics problem with a temporal solving. The topological configuration of the actuator is suitable to a plate assumption for the mechanical analysis. The abrasion shield layer of the wing is represented by a plane plate and the efforts applied to it coming from the conductor lines, as shown in figure 4.

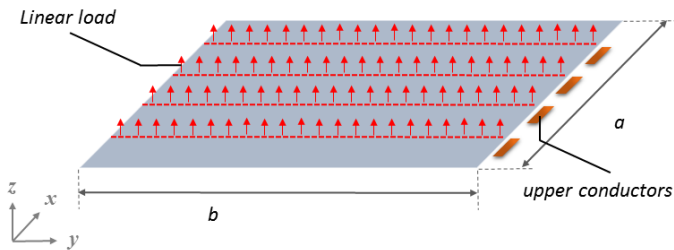


Fig. 4 Metallic plate and applied force density.

Given the characteristics of the activation current impulse, it is possible to calculate the force density generated by the conductors, which is subsequently applied to the plate mechanical model and will enable the calculations for the associated mechanical deformation. The calculation stages integrated in the model and the data transmission among them are listed in figure 5. A calculation chain is done using different programs with connectivity to other program editors, necessary condition for the integration of the final multiphysical model.

MacMMems, an experimental platform for electromagnetic calculations [7], is chosen to host the electromagnetic equations. The MacMMems entities have an *.sml extension, they can be compiled by CADES, an equation editing program that allows creation of *.icar extension components [8]. Icar components can be ran by Matlab® via a dedicated plug-in, opening a large choice of operations. Mechanical expressions are coded in a Matlab function.

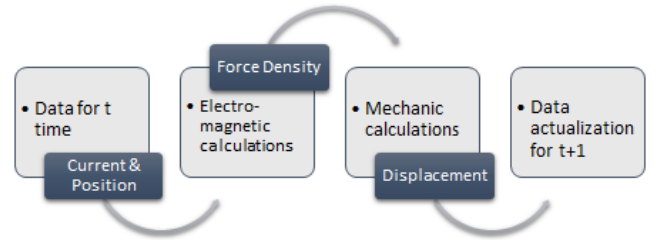


Fig. 5 Data transmission in the multi physics calculation chain.

A Matlab program is conceived to integrate and drive all the cited components. The construction of the calculation blocs is presented in the following sections.

3.1. Electromagnetic model

The deicer operation principle resides on the interaction of electromagnetic forces between two series of conductors. These conductors are rectangular parallelepipeds for which we assume a uniform current density distribution. Such interaction can be described by Biot & Savart (1) and Laplace (2) laws, to estimate the induction flux and the force density.

$$\vec{B}(\vec{r}) = \frac{\mu_0}{4\pi} \iiint \frac{\vec{j} \times (\vec{r} - \vec{r}')}{|\vec{r} - \vec{r}'|^3} dv \quad (1)$$

$$\vec{dF} = \vec{j} dv \times \vec{B} \quad (2)$$

where \vec{B} is the electromagnetic induction (T), \vec{j} the current density (A/m²), \vec{dF} the linear magnetic force density (N/m), dv an elementary volume (m³), r the position of the reference point and r' the position of dv .

3.1.1. PEEC model

In a first time, Laplace forces value was estimated with InCa3D simulation program; a PEEC based method (Partial Element Equivalent Circuit) [9]. For constructing the project, the conductors and the plate geometry are represented in detail as it can be appreciated in figure 6. As this program works in frequency domain while our electric signal is expressed in time domain, mathematical transformations have to be done in both senses. It has been determined that calculations for the first 33 harmonics of the current signal had the most influence, frequency up to 20625Hz, and will be enough to consider a good reconstruction of the results.

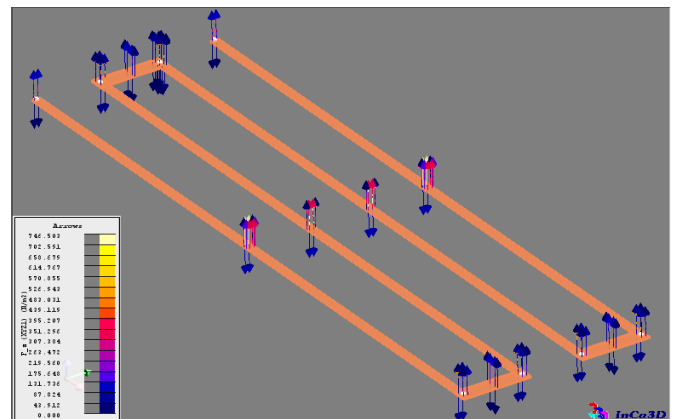


Fig. 6 Representation of Laplace force vectors, from InCa3D.

One important remark is the fact that the forces are concentrated in lines over long conductor sections, what leads to the simplification hypothesis presented in the next section.

3.1.2. Unitary linear conductor hypothesis

Electromagnetic analysis leads to demonstrate that the mutual influence between the different lines of conductors was small enough to simplify the analysis and consider a more single pattern. Only one linear element of the conductor is enough for magnetic calculations, figure 7 shows the evidence when comparing results for analytical and numerical calculations of the magnetic induction field along the X axis.

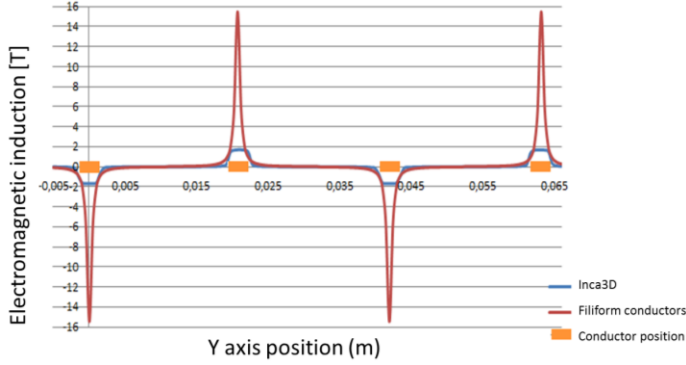


Fig. 7 Electromagnetic induction along X axis for $y=0$.

Simple analytic expressions were established for Laplace force. These expressions were integrated in platform MacMMems platform, simplifying the operation for Laplace forces estimation. Figure 8 shows the simplified conductors arrangement. Results were validated with less than 0.2% of error in comparison to Inca3D simulation results.

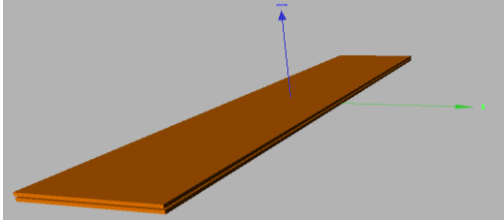


Fig. 8 Representation of two conductors, from MacMMems project.

The weakness of the approach regarding this application, is that MacMMems equations are time independent, so they deliver a static response for a unique value of I in t instant, while magnetic fields evolution for this case is dynamic, due to the electric signal definition $i(t)$. In order to reconstruct dynamics of the magnetic force, a time step is established and evaluations for each t instant are launched via Matlab®.

3.2. Electric model

Toward a complete model, it is crucial to obtain the electric definition for all the system elements. First, the impedance value of the conductors spire is calculated with PEEC method. Results are presented in figure 9, for the significant harmonics.

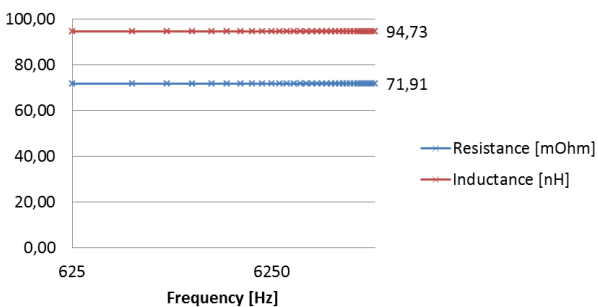


Fig. 9 Resistance and inductance values for all the conductors.

For complete pattern of conductors we have $R=72\text{ m}\Omega$ and $L=95\text{ nH}$. Numeric and analytic results for the resistance value match. When comparing to the calculations of a single conductor line, it can be noticed that parasitic inductance is low due to the self-anti-self effect. It is observed that the values for resistance and inductance are constant for different frequency values. The equivalent electrical scheme for the deicer is detailed in figure 9.

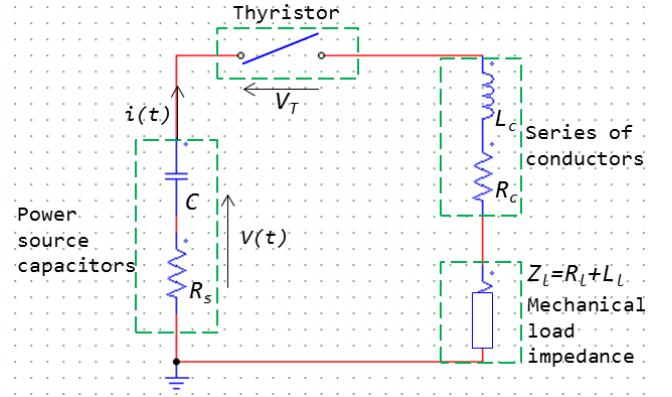


Fig. 9 Electronic schematic of the system elements.

The electric current for this circuit is ruled by a second order differential equation. The resulting expression is expressed by equation (3).

$$i(t) = \frac{V_0 - V_T}{L_{eq}(\alpha_1 - \alpha_2)} (e^{\alpha_1 t} - e^{\alpha_2 t}) \quad (3)$$

$$\begin{cases} \alpha_1 = \frac{-R_{eq}C + \sqrt{R_{eq}^2 C^2 - 4L_{eq}C}}{2L_{eq}C} \\ \alpha_2 = \frac{-R_{eq}C - \sqrt{R_{eq}^2 C^2 - 4L_{eq}C}}{2L_{eq}C} \end{cases} \quad \begin{cases} L_{eq} = L_c + L_l \\ R_{eq} = R_l + R_c + R_s \end{cases}$$

Where V_0 is the initial supply voltage; V_T is the voltage drop in the Thyristor; L_c and L_l are the inductance value for the conductor and the mechanic load (H); R_l , R_c and R_s are the equivalent resistance of the mechanical load, the conductor coil and the power source capacitors, respectively, in (Ω); C is the capacity of the power source capacitors (F). The resulting time constants of the electric signal are $\tau_1 = RC = 147\text{ }\mu\text{s}$, $\tau_2 = L/R = 1.3\text{ }\mu\text{s}$ and $\tau_3 = 2\pi\sqrt{LC} = 86\text{ }\mu\text{s}$.

3.2.1. Energy balance

The impedance value of the mechanical load is evaluated by an energy balance. An analyze of the energy distribution leads to equation (4), which expresses the amount of energy left for mechanic work after Joule losses in conductors and eddy current losses in the aluminum plate. This gives an equivalent expression useful for estimating the value of the load resistance R_{load} .

$$\begin{aligned} E_{meca} &= E_{abs} - E_{Joules} - E_{eddycurrents} \\ &= \sum_i R_{load} * I^2(i\Delta t) * \Delta t \quad (4) \end{aligned}$$

E_{meca} is the energy available to be transformed into mechanical effort (J); E_{abs} the total energy absorbed by the system; E_{Joules} the energy lost by Joule effect in conductors coil and finally $E_{eddycurrents}$ the energy lost by eddy currents produced in the aluminum shield (J).

From numerical integration of the power supply signals we obtain $E_{abs} = 283\text{ J}$ or 1.38 J/cm^2 for the surface of the device

equal to 205.6cm^2 . Concerning Joule losses we have $E_{Joules} = 262.5\text{J}$. Finally, eddy current losses estimation in the aluminum plate is achieved by Inca3D simulation. The figure 10 shows the eddy current distribution inside of the plate for the first harmonic current signal.

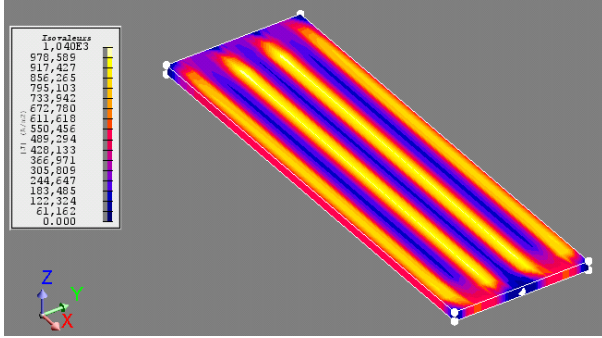


Fig. 10 Generated eddy current distribution in the aluminum abrasion shield.

Total losses by eddy currents are equal to 0.287J or 0.0014J/cm^2 . So, $E_{meca} = 20.2\text{J}$ and a preliminary simplistic estimation of the mechanical impedance to start electric analysis give $R_{load} = 5.7\text{m}\Omega$. All the parameters to reconstruct the model of the electric signal are available. Figure 11 provides the comparison between the analytical model and the measured current signal from industrials' experiments.

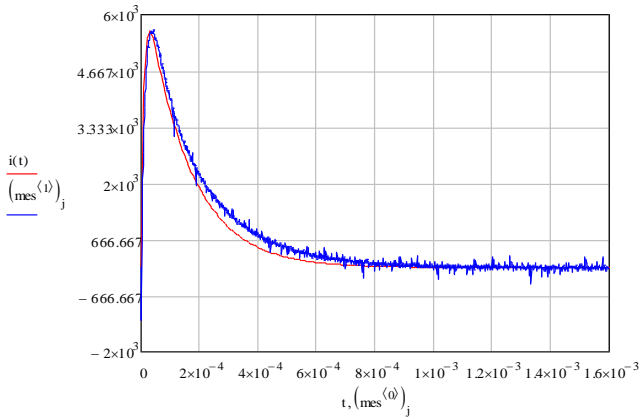


Fig. 11 Power supply current signal, from mathematical expression $i(t)$ and from measurements $mes^{^(t)}$.

Concerning the value of the mechanical load inductance, $L_{load} = 600\text{nH}$ was chosen by fitting the curves. A more accurate value of the mechanical load impedance could be found when all the correlated parts of the multi-physical model will be connected.

3.3. Mechanical model

For the mechanical description, in a preliminary attempt, beam deflection analysis was intended for modeling the abrasion shield deformation but it clearly result a too simplistic solution.

Reconstruction of the deformation behavior from Zodiac prototype measurements, figure 12, clearly shows pics at the position of conductors, valleys at the place where elastomer cylindrical inserts are situated, as well as minimum displacement in the edges of the plate due to boundary conditions. This behavior of the abrasion shield justifies the mechanical resolution of a plate problem.

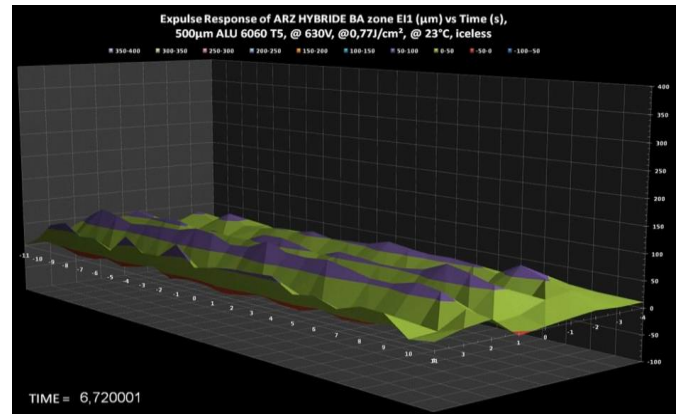


Fig. 12 Displacement of the plate for instant t from measurements [4].

Linear load coming from the magnetic forces over conductor lines are introduced as distributed forces, values come from electromagnetic model. Cylindrical elastomer inserts are considered as punctual forces applied directly to the plate structure in the corresponding position, and are modeled by equivalent springs behavior. Boundary conditions are introduced to describe the type of clamping along the edges. Moreover, elastomer surrounding the rest of the system and other elements will be considered in the general elasticity definition. Rigidity of the conductors is very small compared to that of the aluminum abrasion shield, so it is neglected.

Under the hypothesis of uniform material properties, the deformation of the plate is described by the following differential equation [10-11]:

$$\frac{\partial^4 w(x,y,t)}{\partial x^4} + 2\beta \frac{\partial^4 w(x,y,t)}{\partial x^2 \partial y^2} + \alpha \frac{\partial^4 w(x,y,t)}{\partial y^4} + \frac{\gamma h}{D_x} \frac{\partial^2 w(x,y,t)}{\partial t^2} = \frac{q(x,y,t)}{D_x} \quad (5)$$

with:

$$\alpha = \frac{D_y}{D_x}; \quad \beta = \frac{H_{xy}}{D_x}; \quad H_{xy} = (4D_{xy} + \mu_y D_x + \mu_x D_y)/2;$$

$$D_x = \frac{E_x h^3}{12(1-\mu_x \mu_y)}; \quad D_y = \frac{E_y h^3}{12(1-\mu_x \mu_y)}; \quad D_{xy} = Gh^3/12$$

where $w(x,y,t)$ is the normal displacement of the plate (m); γ the volume mass density (kg/m^3); h the plate thickness (m); μ_x and μ_y Poisson's coefficients; E_x and E_y Young's modulus (GPa), G the shear modulus (GPa), D_x and D_y the flexural rigidities of the orthotropic plate, while D_{xy} represents the torsional rigidity and $q(x,y,t)$ the applied distributed force (N/m). In the aim of acquiring more precision, some other characteristics have been integrated to enhance the model.

3.3.1. Cylindrical elastomer inserts

The proposed model consists on considering each insert as an equivalent spring for which the stiffness constant includes the material and geometrical characteristics. The resulting elastic force is given by relation (6).

$$F_e = k_{eq} * \Delta l \quad (6)$$

where F_e is the equivalent punctual force to be applied at the position of the insert (N), Δl is the total elongation in reference to the initial position (m), and $k_{eq} = \frac{SE_y}{l}$ is the stiffness

(N*m/rad) that considers E_y Young modulus (GPa), l longitude (m) and S section (m²) of the cylindrical insert..

3.3.2. Boundary conditions

The plate edges are submitted to unclear boundary conditions, due to the vulcanization process of the elastomer layers that contain the device. The situation of our plate is between the clamped edge (minimum displacement) and the simply supported edge (maximum displacement). Both cases are treated to frame the result.

3.3.3. Contact forces

It is also necessary to incorporate a restriction on the normal displacement for negative value ($z \leq 0$). Because of the presence of the wing structure, an elastic force is assigned at the instant of contact with the structure, of the same magnitude than the force excessed to the plate but with opposite sense. If displacement becomes negative, it will be canceled by this contact force to ensure that natural mechanical limits are respected.

3.4. Resolution approaches

For solving the differential equation (5) describing the dynamics of the mechanical response, two approaches are put in place. The first one is a static resolution integrated in a loop for reconstructing the deformation curve in function of time. The second one is a finite difference scheme which can estimate with enough accuracy the value of the deformation.

3.4.1. Loop of static resolutions

The static resolution is carried out as part of the strip analysis method [12-13]. This method implies the division of the plate in long sections, and the n number of strips depends on the number of loads and reactions. In each point where an effort is applied, the boundary of one strip element is defined. Equation (5) restricted to its static form is applied to each strip and continuity restrictions are established. This approach is implemented according to the resolution loop explains figure 13.

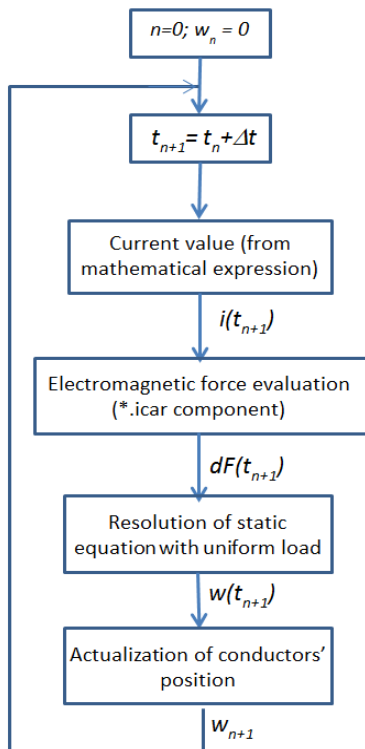


Fig. 13 Description of the static resolution loop.

3.4.2. Finite difference scheme

Precedent resolution strategy is easy to apply but it does not include the dynamic term for the deformation equation (5). Another approach is to employ a numerical resolution based in finite difference scheme [14] with a spatial discretization and a Newmark algorithm due to the presence of a second order time dependent differential equation.

With this approach and considering the plate is the space to be analyzed as an array of multiple points, like that of figure 14, equation (5) can be rewritten as in (7).

$$W_{i,j,k+1} = A \cdot W_{i,j,k} + 2 \cdot W_{i,j,k} - W_{i,j,k-1} + B \cdot F \quad (7)$$

where A is a matrix integrated by the constant coefficients for the points surrounding the current point of analysis, W are the displacement matrices for the element in position i,j at time k ($W_{i,j,k}$), at time $k+1$ ($W_{i,j,k+1}$) and at time $k-1$ ($W_{i,j,k-1}$), B is a constant that multiplies the force vector F containing the efforts.

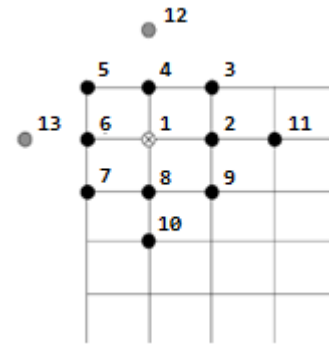


Fig. 14 Elements array for finite difference method.

The displacement for the points that exist outside the plate and the points along the edges, are determined by the boundary conditions (8) and (9). Initial conditions are given by (10).

$$w|_{x=a} = 0 \quad (8)$$

$$\frac{\partial w}{\partial x} \Big|_{x=a} = \frac{1}{2\Delta x} (w_{i+1,j,k} - w_{i-1,j,k}) = 0 \quad (9)$$

$$w_{i,j,k} \Big|_{t=0} = 0 \quad (10)$$

The constructed models are integrated in a code that drives multiple simulation programs. The calculations were done through the static strip model and compared to finite elements method by creating a project in Comsol program. Both approaches match.

To complete the validation of the mechanical model, it is possible to apply the Von mises criterion. This evaluation endorses of the good performance of the system. The coherence is verified as it can be seen in figure 15.

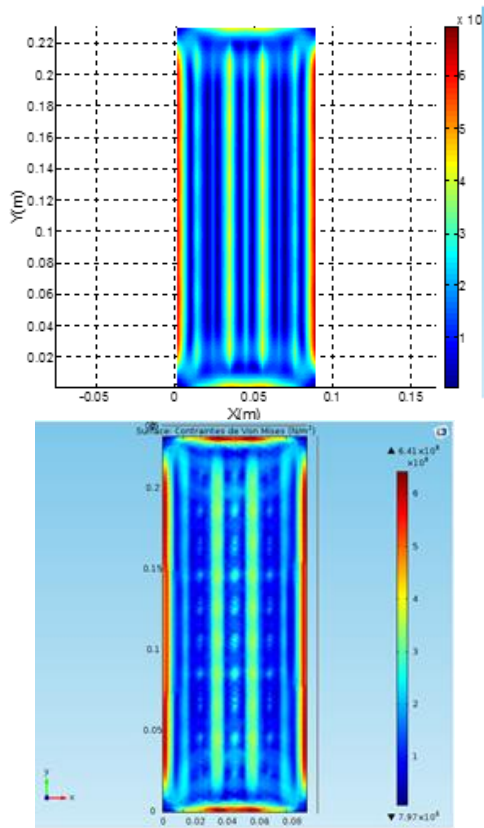


Fig.15_Von Mises criteria evaluated by analytic approach at the (top figure) and finite elements model (bottom figure).

4. RESULTS

During experimental measurements of the industrial partner, displacement on 5 points of the plate was analyzed in detail. These points are shown in figure 16. They are the reference for validating the models. The corresponding measured displacement curves, in function of time, are found in figure 17. It can be appreciated that the dynamics of the mechanical response has a damped vibration behavior.

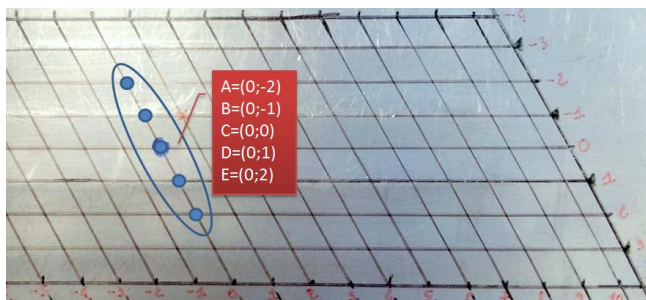


Fig.16 Evaluation points on the abrasion shield or plate [5].

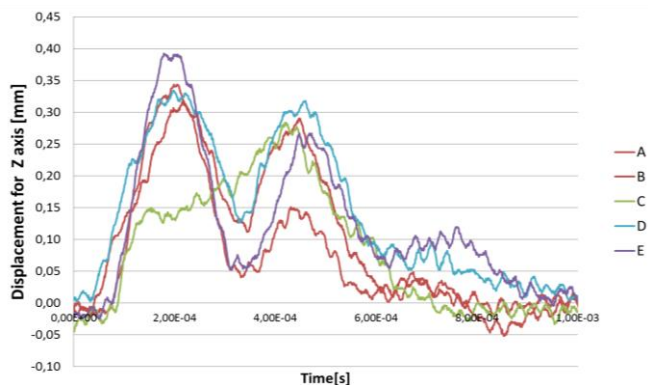


Fig.17 Measurements of displacement for some points of the plate [5].

From electromagnetic model we know the magnitude of the force $F=1252N$ and the force density is $DForce=5620N/m$ for one conductor line feed by the maximum current value $I=5800A$. Icar component, containing the electromagnetic calculations, can be called for each current magnitude on time t . Then, the results are inserted as initial data for the mechanical model.

After so, there are two choices, either to solve by the static loop resolution or with the finite difference scheme. Also, concerning the boundary conditions at the edges, we established two situations, simple supported and clamped joint. The simple supported case will give the maximum displacement of the frame, while the clamped condition will mark the minimum displacement that can be achieved. Curves of figure 18 and 19 correspond to the results of the loop approach. The gap between both initial conditions is very small, 1,01mm for the simple supported versus 1,03mm for the clamped situation. This method reconstructs the dynamics of the mechanical response by a series of static solutions. So, it is natural if dynamics of the curves is not similar to that of measurements of figure 16 but tends to follow the current signal of figure 3 instead.

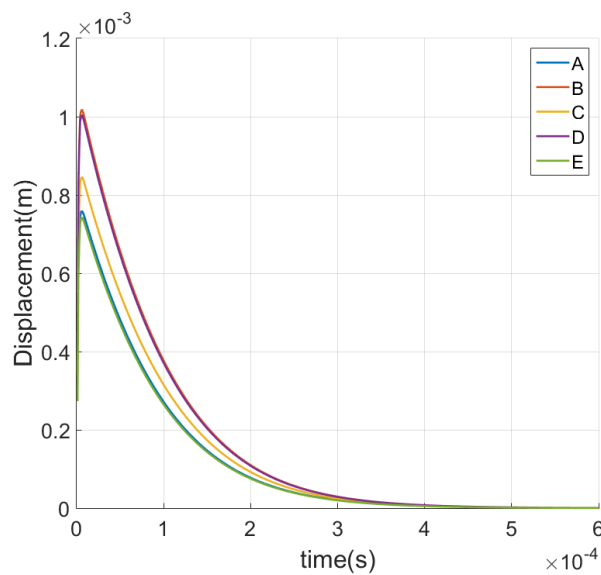


Fig. 18 Displacement results for static resolution, clamped plate edges.

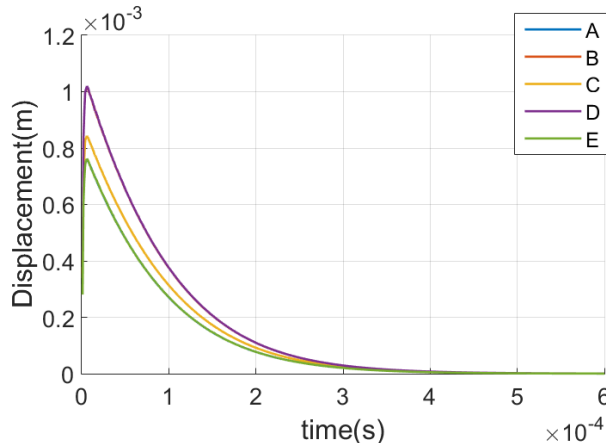


Fig. 19 Displacement results for static resolution, single supported plate edges

In the other hand, curves of figure 20 belong to the displacement in function of time obtained with the finite difference scheme approach. As in this case the term defining the dynamics of the mechanic response is estimated, the results for the displacement of the plate show a vibratory response, smoothly damped, like the real measurements.

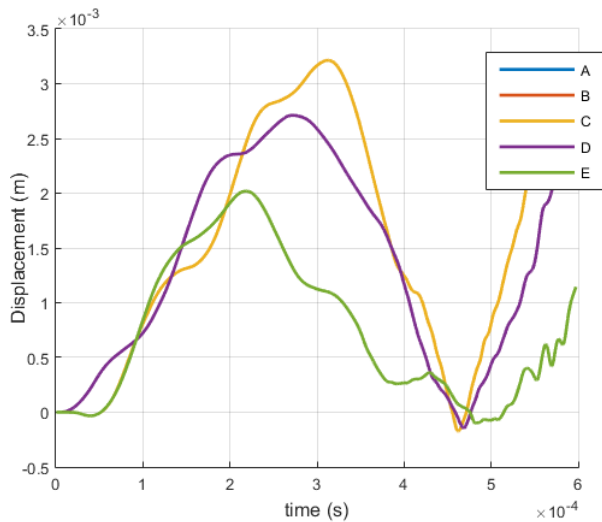


Fig. 20 Displacement curves at point A, B, C, D, E of the plate obtained by resolution with the finite difference scheme.

Comparing the maximum displacements at the same point E for the three cases, in measurements we have that point E presents the maximum displacement of 0.39mm at $t=0.2\text{ms}$, from static solution we obtain a displacement of 0,8mm at $t=0.06\text{ms}$ and finally, with finite differences method we obtain 2mm of displacement at $t= 0.23\text{ms}$. At the actual development state of the approaches, even when the static loop is more accurate in terms of displacement, the dynamics of the mechanical response is better represented by the finite differences method.

The model can still be enhanced by adding more details. However, the plate model seems to be adapted to the problem as it permits to integrate all the characteristics of the device.

5. CONCLUSIONS AND PERSPECTIVES

All the parameters involved to the operation have been modeled; from electrical signal, passing through geometrical characteristics, to mechanical forces and dynamic response. Equivalent electric model of the mechanical load should be reformulated now that many unknown terms have been elucidated. This action should offer more precision and as a consequence, a better perspective of the device operation.

Despite the complications related to solving a time dependent second order differential equation, two solutions were proposed and developed. Sensibility tests and preliminary optimization results point for structural modifications on the device. Optimization stage is still in progress.

As a perspective, both solutions, static loop and finite difference schema, are suitable for optimization procedure what is clearly the next step of our work. ▀

6. REFERENCES

- [1] X. Roboam, B. Sareni and A. De Andrade, "More Electricity in the Air: Toward Optimized Electrical Networks Embedded in More-Electrical Aircraft" IEEE Industrial Electronics Magazine, vol. 6, 6-17, 2012.
- [2] E. Belot, S. Le Garrec and A. Delehelle, "Dossier de Définition Technique d'un Actionneur Expulse", Zodiac Aerospace, Inter-technical Report 7N-17211, Jul. 2013.
- [3] C. Laforte, J.L. Laforte, "Deicing Strains and Stresses of Iced Substrates", Journal of adhesion science & technology, 26:4-5, 603-620, Leiden 2012.C.
- [4] Lange et al., "Paschen Problems in Large Coil Systems", IEEE Transactions on applied superconduvivity, Vol. 22, No. 3, June 2012.
- [5] Zodiac Aerospace, "RecapMesuresEI2_UID_1.exe", Inter-technical Report 7N-17211, 2013.
- [6] S. Le Garrec et al. "Spécification d'un actionneur électromécanique", Zodiac Aerospace, Inter-technical Report 7N-17079, Oct. 2013.
- [7] HL Rakotoarison et al., "Formal sensitivity computation of magnetic moment method", IEEE Transactions on Magnetics 44 (6), June 2008.
- [8] P. Pham Quang et al. "Semi-Analytical Mag neto-Mechanic Coupling With Contact Analysis is for MEMS/NEMS", IEEE transactions on magnetics, vol. 47, no. 5, may 201.
- [9] Edith Clavel et al. "Far Field Extrapolation from Near Field Interactions and Shielding Influence Investigations Based on a FE-PEEC Coupling Method", Electronics 2013, 2.
- [10] E. Ventsel, T. Krauthammer "Thin Plates and Shells: Theory, Analysis, and Applications", Marcel Dekker, Inc., Basel, Switzerland, 2001.
- [11] Timoshenko S. and W. Woinowsky-Kreiger, "Theory of plates and shells", Mc.GrawHill 1959.
- [12] I.E. Harik and G.L. Salamoun, " The analytical strip method of solution for stiffened rectangular plates", Computers & Structures, vol. 29, No. 2, pp. 283-2 91, 1988 .
- [13] I.E. Harik, X. Liu and N. Balakrishnan, "Analytical solution to free vibration of rectangular plates", Journal of Soud and Vibration (1992), 153(1), 51-62.
- [14] A.R.Tavakolpour, I.Z.Mat Darus, M. Mailah, "Numerical simulation of a flexible plate system for vibration control", WSEAS Transactions on systems and control, Issue 3, Volume 4, 2009.